

---

*This copy is for your personal, non-commercial use only.*

---

If you wish to distribute this article to others, you can order high-quality copies for your colleagues, clients, or customers by [clicking here](#).

Permission to republish or repurpose articles or portions of articles can be obtained by following the guidelines [here](#).

**The following resources related to this article are available online at [www.sciencemag.org](http://www.sciencemag.org) (this information is current as of August 28, 2011):**

**Updated information and services**, including high-resolution figures, can be found in the online version of this article at:

<http://www.sciencemag.org/content/326/5955/966.full.html>

A list of selected additional articles on the Science Web sites **related to this article** can be found at:

<http://www.sciencemag.org/content/326/5955/966.full.html#related>

This article **cites 17 articles**, 6 of which can be accessed free:

<http://www.sciencemag.org/content/326/5955/966.full.html#ref-list-1>

This article has been **cited by** 7 article(s) on the ISI Web of Science

This article has been **cited by** 3 articles hosted by HighWire Press; see:

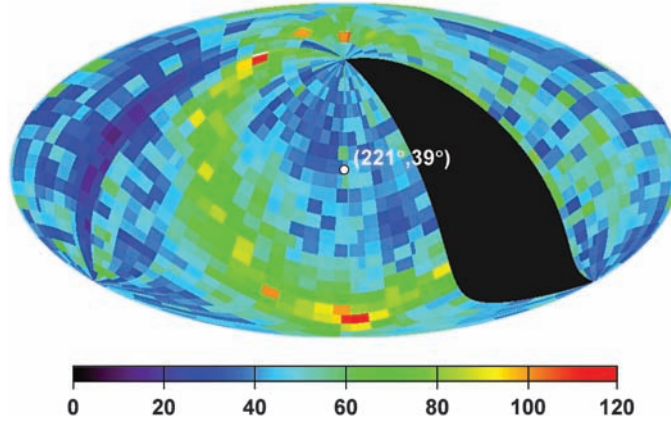
<http://www.sciencemag.org/content/326/5955/966.full.html#related-urls>

This article appears in the following **subject collections**:

Planetary Science

[http://www.sciencemag.org/cgi/collection/planet\\_sci](http://www.sciencemag.org/cgi/collection/planet_sci)

**Fig. 3.** The product of the ion pressure  $\Delta P_{\text{ion}}$  in the heliosheath and the radial thickness  $L$  of the ENA emission in units of p dynes  $\text{cm}^{-2}$  AU over the energy range from 0.2 to 6 keV that includes the 0.44-keV passband of IBEX-Lo and the 0.7-, 1.1-, 1.7-, 2.7-, and 4.3-keV passbands of IBEX-Hi. The black swath is data removed because of poor statistics in the IBEX-Lo energy passband.



sistent with the locus of points for which the external LISM magnetic field vector lies transverse to the IBEX LOS, a region of comparably strong dynamic and magnetic force exerted by the LISM (6, 8). The likely LOS direction  $(\lambda, \beta) = (221^\circ, 39^\circ)$  parallel to the interstellar magnetic field derived here lies within the range  $210^\circ \leq \lambda \leq 240^\circ$  and  $30^\circ \leq \beta \leq 60^\circ$ , obtained using the offset in flow directions between interstellar  $\text{H}^0$  and  $\text{He}^0$  (14), and is consistent with the direc-

tion inferred from 2- to 3-kHz radio emissions measured at the Voyager spacecraft (15).

**References and Notes**

1. M. Gruntman, *Rev. Sci. Instrum.* **68**, 3617 (1997).
2. M. Gruntman et al., *J. Geophys. Res.* **106**, 15767 (2001).
3. S. A. Fuselier et al., *Space Sci. Rev.*, 10.1007/s11214-009-9495-8 (2009).
4. H. O. Funsten et al., *Space Sci. Rev.*, 10.1007/s11214-009-9504-y (2009).

5. D. J. McComas et al., *Space Sci. Rev.*, 10.1007/s11214-009-9499-4 (2009).
6. D. J. McComas et al., *Science* **326**, 959 (2009); published online 15 October 2009 (10.1126/science.1180906).
7. S. A. Fuselier et al., *Science* **326**, 962 (2009); published online 15 October 2009 (10.1126/science.1180981).
8. N. A. Schwadron et al., *Science* **326**, 966 (2009); published online 15 October 2009 (10.1126/science.1180986).
9. R. B. Decker et al., *Nature* **454**, 67 (2008).
10. D. J. McComas et al., *Geophys. Res. Lett.* **25**, 1 (1998).
11. N. A. Schwadron, D. J. McComas, *Geophys. Res. Lett.* **30**, 1587 (2003).
12. B. G. Lindsay, R. F. Stebbings, *J. Geophys. Res.* **110**, A12213 (2005).
13. H. R. Muller, G. P. Zank, *J. Geophys. Res.* **109**, A07104 (2004).
14. R. Lallement et al., *Science* **307**, 1447 (2005).
15. D. A. Gunnert, W. S. Kurth, I. H. Cairns, J. Mitchell, *AIP Conf. Proc.* **858**, 129 (2006).
16. We thank all the IBEX team members, who enabled the success of IBEX through their individual talents, dedication, and hard work. This work was funded by the NASA Explorer Program. Work at Los Alamos was performed under the auspices of the U.S. Department of Energy.

21 August 2009; accepted 2 October 2009  
 Published online 15 October 2009;  
 10.1126/science.1180927  
 Include this information when citing this paper.

# Comparison of Interstellar Boundary Explorer Observations with 3D Global Heliospheric Models

N. A. Schwadron,<sup>1,13\*</sup> M. Bzowski,<sup>2</sup> G. B. Crew,<sup>3</sup> M. Gruntman,<sup>4</sup> H. Fahr,<sup>5</sup> H. Fichtner,<sup>6</sup> P. C. Frisch,<sup>7</sup> H. O. Funsten,<sup>8</sup> S. Fuselier,<sup>9</sup> J. Heerikhuisen,<sup>10</sup> V. Izmodenov,<sup>11</sup> H. Kucharek,<sup>12</sup> M. Lee,<sup>12</sup> G. Livadiotis,<sup>13</sup> D. J. McComas,<sup>13,14</sup> E. Moebius,<sup>12</sup> T. Moore,<sup>15</sup> J. Mukherjee,<sup>13</sup> N.V. Pogorelov,<sup>10</sup> C. Prested,<sup>1</sup> D. Reisenfeld,<sup>16</sup> E. Roelof,<sup>17</sup> G.P. Zank<sup>10</sup>

Simulations of energetic neutral atom (ENA) maps predict flux magnitudes that are, in some cases, similar to those observed by the Interstellar Boundary Explorer (IBEX) spacecraft, but they miss the ribbon. Our model of the heliosphere indicates that the local interstellar medium (LISM) magnetic field ( $B_{\text{LISM}}$ ) is transverse to the line of sight (LOS) along the ribbon, suggesting that the ribbon may carry its imprint. The force-per-unit area on the heliopause from field line draping and the LISM ram pressure is comparable with the ribbon pressure if the LOS  $\sim 30$  to 60 astronomical units and  $B_{\text{LISM}} \sim 2.5$  microgauss. Although various models have advantages in accounting for some of the observations, no model can explain all the dominant features, which probably requires a substantial change in our understanding of the processes that shape our heliosphere.

Previous models of energetic neutral atom (ENA) maps ( $I$ ) provide limits on possible emission patterns depending on the assumed proton distributions in the heliosheath. Models with assumed Maxwellian distributions in the heliosheath show a broad enhanced emission region near the nose where the flow stagnates, whereas highly nonthermal distributions dominated by pickup ions (PUIs) show higher intensities in the sidewind direction and toward

the tail where the line-of-sight (LOS) integrations across the heliosheath extended over large distances [hundreds of astronomical units (AU)]. Three-dimensional (3D) models incorporating a  $\kappa$  distribution, defined in (2), as a distribution with a Gaussian-like core and a power-law tail, manifest structure influenced by the local interstellar medium (LISM) magnetic field ( $B_{\text{LISM}}$ ) (3). The observed difference inside the termination shock (TS) between in-

terstellar helium flow and the hydrogen flow (4), which interacts more strongly with the outer heliosheath plasma (beyond the heliopause), suggests that  $B_{\text{LISM}}$  lies in the plane of the two flow vectors (the hydrogen deflection plane), which can push the TS closer to the Sun in the Southern Hemisphere, helping to explain why Voyager 2 (V2;  $-29^\circ$  latitude) crossed the TS  $\sim 10$  AU closer to the Sun than

<sup>1</sup>Department of Astronomy, Boston University, Boston, MA 02215, USA. <sup>2</sup>Space Research Centre of the Polish Academy of Sciences, 00-716 Warsaw, Poland. <sup>3</sup>Kavli Institute, Massachusetts Institute of Technology, Cambridge, MA 02139, USA. <sup>4</sup>Astronomical Engineering Division, University of Southern California, Los Angeles, CA 90089, USA. <sup>5</sup>Institut für Astrophysik und Extraterrestrische Forschung, University of Bonn, 53115 Bonn, Germany. <sup>6</sup>Institut für Theoretische Physik IV, Ruhr-Universität Bochum, 44780 Bochum, Germany. <sup>7</sup>Department of Astronomy and Astrophysics, University of Chicago, Chicago, IL 60637, USA. <sup>8</sup>Los Alamos National Laboratory, Los Alamos, NM 87545, USA. <sup>9</sup>Lockheed Martin Advanced Technology Center, Palo Alto, CA 94304, USA. <sup>10</sup>Department of Physics, University of Alabama, Huntsville, Alabama 35805, USA. <sup>11</sup>Department of Aeromechanics and Gas Dynamics, Moscow State University, and Space Research Institute (IKI) and Institute for Problems in Mechanics Russian Academy of Sciences, 117997 Moscow, Russia. <sup>12</sup>Department of Physics, University of New Hampshire, Space Science Center, Durham, NH 03824, USA. <sup>13</sup>Department of Space Science and Engineering, Southwest Research Institute, San Antonio, TX 78228, USA. <sup>14</sup>Department of Physics, University of Texas at San Antonio, San Antonio, TX 78249, USA. <sup>15</sup>NASA Goddard Space Flight Center, Greenbelt, MD 20771, USA. <sup>16</sup>Department of Physics, University of Montana, Missoula, MT 59812, USA. <sup>17</sup>Applied Physics Laboratory, Johns Hopkins University, Laurel, MD 20723, USA.

\*To whom correspondence should be addressed. E-mail: nathanas@bu.edu

did Voyager 1 (V1; 34° latitude) (5–8). Here, we compare Interstellar Boundary Explorer (IBEX) observations (9–11) with sophisticated models of the heliosphere and outline considerations in the development of new concepts to understand the ribbon.

The ENA flux observed by IBEX derives from the LOS integral over the charge-exchange probability for the differential intensity of protons that move radially inward toward the Earth as they gyrate about the field. ENAs experience charge-exchange and photo-ionization losses as they propagate through the supersonic solar wind and are deflected and shifted in energy by the Sun’s gravity and radiation pressure. At the energies considered here (~0.4 to 4 keV), these are small effects (at 0.4 keV, the ionization loss is ~40%, deflection is ~0.5°, and energy shift is ~2%) that decrease with energy. The ENA distribution at 1 AU is sensitive to the LOS path along which emission occurs, the density and bulk motion of the heliosheath plasma, and the energy and pitch-angle distributions of the source proton population.

We simulated ENA maps using different models with different assumptions for the local interstellar conditions. Model 1 (3) uses a magnetohydrodynamic (MHD) model ( $B_{LISM} = 1.8 \mu\text{G}$ ) (8) incorporating a  $\kappa$  distribution (with  $\kappa = 1.6$ ) throughout the heliosheath with the derived MHD plasma parameters, but assumes a uniform density of interstellar hydrogen ( $0.1 \text{ cm}^{-3}$ ) a posteriori to generate ENAs and does not treat the interaction between the plasma and neutrals self-consistently. Model 2 (Fig. 1) (12) uses an MHD model that self-consistently treats the charge-exchange interaction between neutral atoms from the LISM and protons that have a  $\kappa$ -function distribution of  $\kappa = 1.6$  inside the heliopause but a Maxwellian distribution outside. The model assumes a 450 km/s solar wind emitted inside the TS and a  $3 \mu\text{G}$   $B_{LISM}$  in the hydrogen deflection plane, tilted by 30° to the LISM flow. There are few structural differences at 1.1 and 4.4 keV (Fig. 1, A and B), indicating that global heliospheric structure, rather than energy-dependent heating, determines the modeled maps. Other sophisticated models incorporating the self-consistent interactions between the heliosheath plasma and LISM neutrals have been run for a range of LISM and solar wind conditions, revealing considerable variability in global structure and dynamics (13).

The features detected by IBEX may be separated into two parts: the ribbon and distributed emissions outside the ribbon. Models currently miss the ribbon. We compared observations (9–11) with simulated fluxes (Table 1) in ~20° regions outside the ribbon. The IBEX fluxes were interpolated to 0.44, 1, and 4 keV in the Sun-centered inertial reference frame. The model fluxes differ substantially from observations by ~6 to 200%. Models also show that the time-varying latitudinal structure of the solar wind may cause 11-year quasi-periodic variations of

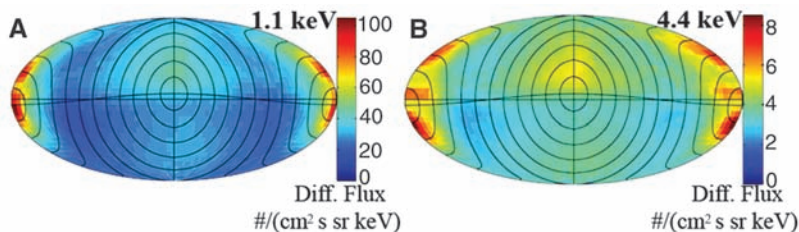
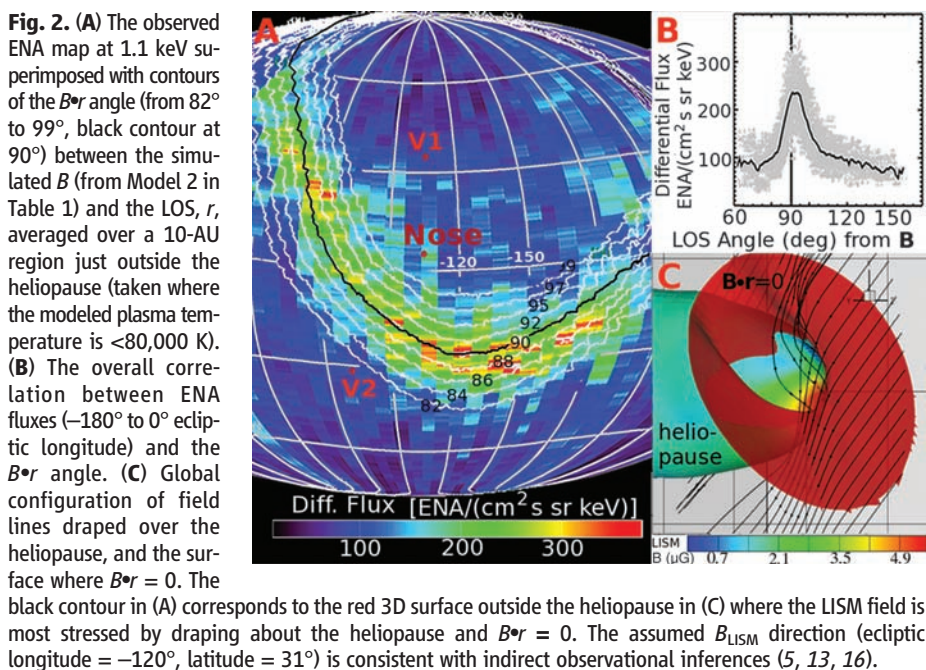


**Fig. 1.** Simulated ENA maps (Mollweide projection) using Model 2 show incident 1 AU ENA fluxes at 1.1 keV (A) and 4.4 keV (B).

**Table 1.** Observed and simulated ENA Fluxes at 0.44, 1 and 4 keV, respectively.

Source	IBEX	Model 1 (3)	Model 2 (12)
	ENAs/(cm <sup>2</sup> s sr keV)	ENAs/(cm <sup>2</sup> s sr keV) (percent relative to IBEX observations)	
Nose	470	230 (49%)	150 (31%)
	96	60 (63%)	43 (45%)
	9	6 (67%)	5.6 (62%)
Tail	530	30 (6%)	360 (68%)
	120	17 (14%)	100 (83%)
	4	4 (100%)	8 (200%)
North Pole	410	150 (37%)	110 (28%)
	76	45 (59%)	34 (45%)
	9	5 (56%)	4 (48%)
South Pole	360	130 (36%)	89 (25%)
	70	40 (57%)	30 (43%)
	9	5 (56%)	4 (44%)
Right flank (longitude = -165°)	230	190 (83%)	110 (48%)
	70	50 (71%)	35 (50%)
	6	5 (83%)	4.3 (72%)
Left flank (longitude = -45°)	380	170 (45%)	110 (30%)
	86	46 (53%)	33 (38%)
	7	5 (71%)	4.3 (61%)



ENA fluxes (14) with a local maximum around 60° latitude for 1 keV ENAs (15).

Model 2 shows correlation between the ribbon and the locus of  $B \cdot r = 0$ , where  $B$  denotes the draped field outside the heliopause and  $r$  is the radial vector along the LOS (Fig. 2). Notwithstanding the assumed direction and strength of  $B_{LISM}$ , the correlation with the  $B \cdot r = 0$  locus suggests that the ribbon may carry the imprint of  $B_{LISM}$  via physical processes not identified in current models.

To quantify the implications of the ribbon for global models, we computed the plasma pressure ( $P$ ) in the ribbon. Direct analysis of the observed fluxes yields  $P \cdot \text{LOS} \sim 100$  AU-pdyne/cm<sup>2</sup> (11). The ribbon's observed width (10) of  $\sim 50$  AU for a heliopause distance 150 AU from the Sun yields  $\text{LOS} \sim 50$  AU, assuming comparable width and depth. This 50 AU LOS suggests  $P \sim 2$  pdyne/cm<sup>2</sup>, 2.5 times the LISM ram pressure (16). We computed a crude model to estimate the increase in pressure ahead of the heliopause caused by the external  $J \times B$  force (where  $J$  is the current density) and thermal pressure [approximated by the dynamical pressure for a LISM proton density of 0.07 cm<sup>-3</sup> and a flow speed of 26 km/s (16)] (Fig. 3). We approximated the heliopause as a perfectly conducting sphere with a slightly flared external magnetic field, conceptually similar to (17) and figure 4C in (9). The crude model compressed  $|B|$  to  $\sim 4$   $\mu\text{G}$  outside the heliopause for  $B_{LISM} = 2.5$   $\mu\text{G}$ . The analytic approach was validated against MHD simulations in other applications (18) and provides the net MHD forces acting on the sur-

face by collapsing current onto the conducting sphere. A ring of high pressure centered on  $B_{LISM}$  is associated with magnetic field line draping. If  $P$  is comparably high, then the LOS is approximately 60 to 30 AU.

Field-draping around the heliopause also compresses the heliosheath plasma, which could enhance ENA emission because of density enhancement (the plasma density,  $n$ , scales with the field strength,  $B$ ) and first adiabatic invariance ( $v_{\perp}^2/B = \text{const}$ , where  $v_{\perp}$  is the velocity of plasma protons perpendicular to the field), provided that some mechanism creates a large suprathermal population beyond the heliopause and there is limited scattering. We assumed a  $\kappa$ -distribution ( $\kappa = 1.6$ ) in the unperturbed LISM, applied  $n/B$  and  $v_{\perp}^2/B$  conservation, and integrated along the LOS from the heliopause to 40 AU beyond it in order to estimate ENA emission (Fig. 3). The structure of the map is preserved at different energies with only the absolute fluxes changing. If distributions are isotropic because of scattering, adiabatic heating and density compression could still enhance fluxes, but the emission band broadens because of the lack of pitch-angle dependence.

Our crude model does not explain the origin of the ribbon but supports the notion that the draped LISM magnetic field influences the heliosheath pressures and ENA emission. Our crude model suggests that the flow may stagnate along the ribbon (9). However, the  $J \times B$  forces that we isolated are present in all MHD models, and stagnation along the  $B \cdot r = 0$  locus is not seen. Therefore, if the  $J \times B$  forces lead to an enhanced ribbon pressure, they must do so

via mechanisms not currently present in global models. For example, elevated  $J \times B$  forces could induce an interchange instability near the heliopause, causing the higher-pressure plasma inside the heliopause to displace field lines longitudinally and protrude beyond the heliopause and elevating ENA emission through charge-exchange with the higher neutral density beyond the heliopause (16) and the lengthened LOS. This instability could depend critically on highly mobile ions, effectively enhancing the pressure along the protruding plasma fingers and highlighting the importance of ion-kinetic effects that are not self-consistently included in current models.

Model predictions provide mixed agreement with observations, and the ribbon is not predicted. The ribbon suggests a high-pressure region in the heliosheath possibly imprinted by the influence of the LISM magnetic field. However, current models are unable to translate the influence of LISM magnetic field into enhanced ENA fluxes along the ribbon, indicating that an important physical ingredient is missing.

References and Notes

1. M. Gruntman *et al.*, *J. Geophys. Res.* **106**, 15767 (2001).
2. V. M. Vasyliunas *et al.*, *J. Geophys. Res.* **73**, 2839 (1968).
3. C. Prested *et al.*, *J. Geophys. Res.* **113**, 6102 (2008).
4. R. Lallement *et al.*, *Science* **307**, 1447 (2005).
5. E. C. Stone *et al.*, *Science* **309**, 2017 (2005).
6. J. D. Richardson *et al.*, *Nature* **454**, 63 (2008).
7. M. Opher *et al.*, *Astrophys. J.* **640**, L71 (2006).
8. M. Opher, E. C. Stone, T. I. Gombosi, *Science* **316**, 875 (2007).
9. D. J. McComas *et al.*, *Science* **326**, 959 (2009); published online 15 October 2009 (10.1126/science.1180906).
10. S. A. Fuselier *et al.*, *Science* **326**, 962 (2009); published online 15 October 2009 (10.1126/science.1180981).
11. H. O. Funsten *et al.*, *Science* **326**, 964 (2009); published online 15 October 2009 (10.1126/science.1180927).
12. N. V. Pogorelov *et al.*, *Astrophys. J.* **695**, 31 (2009).
13. V. Izmodenov, D. Alexashov, A. Myasnikov, *Astron. Astrophys.* **437**, 35 (2005).
14. K. Scherer, H.-J. Fahr, *Geophys. Res. Lett.* **30**, 1045 (2003).
15. O. Sternal, H. Fichtner, K. Scherer, *Astron. Astrophys.* **477**, 365 (2008).
16. P. C. Frisch *et al.*, in *The IBEX Mission*, D. J. McComas, N. A. Schwadron, G. Zank, Eds. (Springer, Dordrecht, Netherlands, 2009), chap. 9, pp. 28–66 (2009).
17. E. N. Parker, *Astrophys. J.* **134**, 20 (1961).
18. P. Wu *et al.*, *J. Geophys. Res.* **113**, A00B05 (2008).
19. We thank the many dedicated people who have made IBEX a success. Special thanks to K. Goodrich, J. Siegel, K. Maynard, and M. Schwadron for their help. This work was primarily supported by the IBEX program.

24 August 2009; accepted 2 October 2009

Published online 15 October 2009;

10.1126/science.1180986

Include this information when citing this paper.

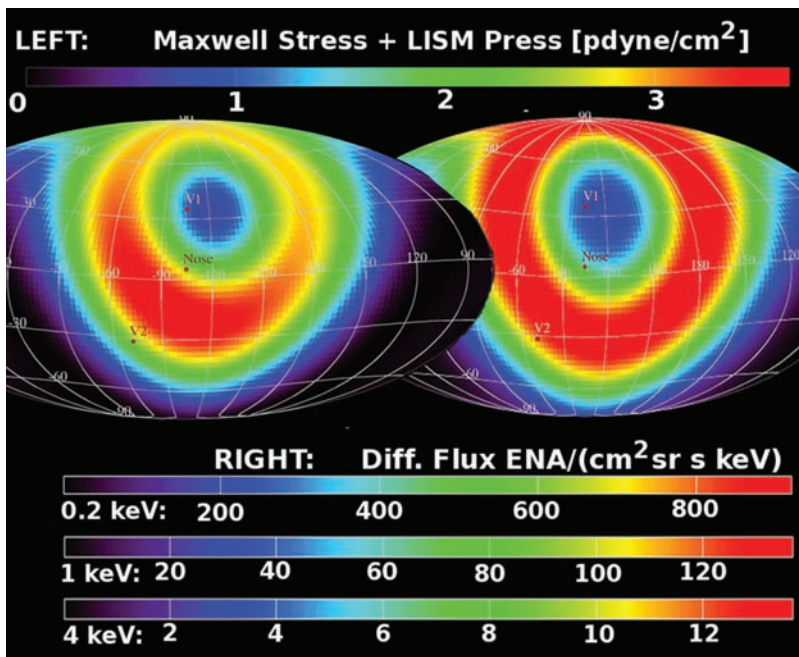


Fig. 3. (Left) Results of a crude model for the combined force-per-unit area on the heliopause from external  $J \times B$  forces (Maxwell stress). (Right) Estimated ENA emission from beyond the heliopause using a crude model of plasma compression.